

Magma–host interactions during differentiation and emplacement of a shallow-level, zoned granitic pluton (Tarçouate pluton, Morocco): implications for magma emplacement

P. Barbey^a, H. Nachit^b and J. Pons^c

^a CRPG-CNRS, B.P. 20, 54501 Vandoeuvre Cedex, France

^b Département des Sciences de la Terre, Université Ibnou Zohr, B.P. 28/S, Agadir, Morocco

^c Laboratoire de Géologie Structurale, UMR-6530, Université d'Orléans, B.P. 6759, 45067 Orléans Cedex, France – remplacé par UMR6113

Abstract

The Tarçouate pluton (Anti-Atlas, Morocco) is an inversely zoned laccolith emplaced 583 Ma ago into low-grade metasediments, with the following succession: leucocratic granites, biotite–granodiorites (\pm monzodiorites), hornblende–granodiorites (\pm monzodiorites) and monzodiorites syn-plutonic dykes. These rocks form two distinct, chemically coherent, units:

(1) A main unit consists of layered ($57 < \text{SiO}_2 < 59$ wt.%) and homogeneous ($63 < \text{SiO}_2 < 67\%$) hornblende–granodiorites, biotite–granodiorites ($67 < \text{SiO}_2 < 72\%$) and aplites ($70 < \text{SiO}_2 < 76\%$). All these rocks are metaluminous to peraluminous and display fractionated HREE depleted patterns ($\text{La}/\text{Yb}_N = 14\text{--}61$; $\text{Yb}_N = 0.7\text{--}6.8$). Initial $^{87}\text{Sr}/^{86}\text{Sr}$ ratios (0.7072 to 0.7080) increase, whereas $\epsilon_{\text{Nd}(t)}$ values (-1.7 to -2.8) decrease from the hornblende– to the biotite–granodiorites. Monzodiorites occur as mafic microgranular enclaves or syn-plutonic dykes.

(2) A subordinate unit consists of leucocratic, distinctly peraluminous, muscovite-bearing granites ($72 < \text{SiO}_2 < 75\%$) occurring at the northern edge of the pluton and as dykes in the surrounding schists towards the top of the pluton. These rocks are free of monzodioritic enclaves. They display less fractionated patterns with higher HREE contents ($\text{La}/\text{Yb}_N = 2\text{--}19$; $\text{Yb}_N = 11\text{--}18$), a distinct $\epsilon_{\text{Nd}(t)}$ value (-11.8) and a $^{87}\text{Sr}/^{86}\text{Sr}$ initial ratio (0.7480) within those of the surrounding schists (0.7393–0.7819).

Magma–host interactions are closely related to differentiation and occurred at different levels, but mainly before emplacement. Field relationships and petrogenetic modelling show that the bt–granodiorites formed at levels deeper than the level of emplacement, by fractional crystallisation ($0.65 < F < 0.85$) with limited amounts of contamination by crustal material (~ 5 wt.%). The hbl–granodiorites differentiated at the level of emplacement by fractional crystallisation leading to residual melts ($F = 0.55$) slightly contaminated by the country rocks (~ 2 wt.%) and represented by aplite dykes. The leucocratic granites are likely to derive by partial melting of lithologies similar in composition to the country metasediments.

These data preclude any significant material transfer process for the emplacement of the Tarçouate pluton, but rather suggest assembly of successive pulses of variably differentiated crystal-poor magmas. These shallow level granitic plutons can be considered as an end-member of magma emplacement with minimum interactions with the country rocks.

Author Keywords : Morocco; Anti-Atlas; Pluton; Granodiorite; Emplacement; Assimilation–fractional crystallisation

1. Introduction

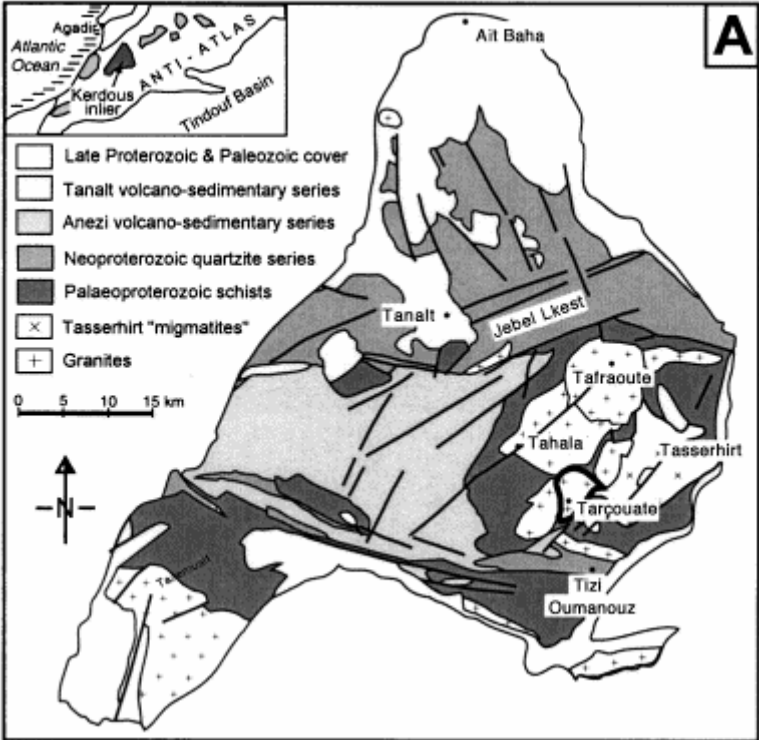
Although the nature and chemical composition of the rock suites forming zoned plutons are closely dependant on processes at the source, they may reflect, to some extent, differentiation and emplacement processes and interactions with the country rocks as well. In other words, should zoned plutons be considered as the locus wherein magma differentiates and interacts with the country rocks, or alternatively, are they simply the assembly of distinct batches differentiated at deeper levels with low interactions with the country rocks? It was shown, for instance, that emplacement of lower crustal magmas in the upper middle crust may lead to strong magma–host interactions with development of wide anatectic aureoles around magma bodies, and significant mingling and mixing (e.g., Williamson and Barbey). In the same way, the crustal exchange process, invoked in the case of plutons emplaced at shallow levels in arcs (Paterson et al., 1996), implies that a significant fraction of the downwards transferred country rocks interacts with magmas and could be assimilated by them. These magma–host interactions may lead to a suite of differentiated rocks by assimilation–fractional crystallisation (AFC; DePaolo and Reiners). However, if magmas emplace at shallow levels along a crustal magma trap by expanding along rheological discontinuities and upheaval of the rock cover (Clemens; Hogan and Vigneresse), magma–host interactions can be expected to be much less intense than in the former situation. Magma–host interactions (both physical and chemical) being dependant on the mechanisms and conditions of magma ponding into the crust, we have, therefore, a way to constrain more tightly the mechanisms of emplacement and differentiation of plutons.

This study based on the Tarçouate pluton (Anti-Atlas, Morocco), intends to discuss the mechanisms of differentiation and emplacement of shallow level zoned granitic plutons from petrological and geochemical points of view. After a presentation of the mineralogy, major- and trace-element chemistry and Sr–Nd isotopic composition of the granitoids and related rocks, the following two points will be addressed: (i) should these plutons be considered simply as an assembly of formerly differentiated magma batches, or is there any evidence of in situ differentiation; and (ii) what is the extent of interactions between magma and host at the level of emplacement?

2. Geological setting

The Proterozoic terrains of the western Anti-Atlas (Morocco) are considered to result from two superposed orogens (Choubert; Charlot and Hassenforder): Palaeoproterozoic (Precambrian I in the local terminology) and Neoproterozoic (Pan-African or Precambrian II). They crop out in several inliers within the Phanerozoic cover and consist of Palaeoproterozoic low-grade metasedimentary series intruded by both Palaeo- and Neoproterozoic granitoids. These rocks are overlain by locally thick Late Proterozoic volcanics and sediments (Precambrian III). The geodynamic evolution of the northern margin of the West-African craton during the Pan-African has been the subject of numerous papers to which the reader is referred for details (e.g. Leblanc; Saquaque; Hefferan; Leblanc; Villeneuve and Ikenne). Briefly, the Kerdous area corresponded during the Pan-African to a continental domain in the rear of a subduction zone, in a situation possibly similar to that of the batholith of Central Patagonia (Rapela and Pankhurst, 1996).

The Tarçouate pluton crops out in the middle part of the Kerdous inlier (Fig. 1A) which consists mainly of a weakly deformed low-grade schist series (metaturbidites). The metasedimentary unit is intruded by several granite plutons of both Palaeoproterozoic (e.g. Tahala dated at 1988 ± 41 Ma, whole-rock Rb–Sr; Charlot, 1982) and Pan-African ages (e.g. Tarçouate: 583 ± 11 Ma, zircon U–Pb data; Aït Malek et al., 1998). The regional structures correspond to WNW–ESE-trending open folds associated with a faint axial plane schistosity. Poikiloblasts of biotite, andalusite and garnet overprint early low-grade assemblages (e.g. Qtz+Ms+Chl) in the thermal aureole around plutons (Nachit et al., 1996). The crystallisation–deformation relationships allow the Palaeoproterozoic granites to be defined as syntectonic (e.g. Tahala, Jebel Ouharen), and the Pan-African ones as post-tectonic (e.g. Tarçouate, Taфраoute).



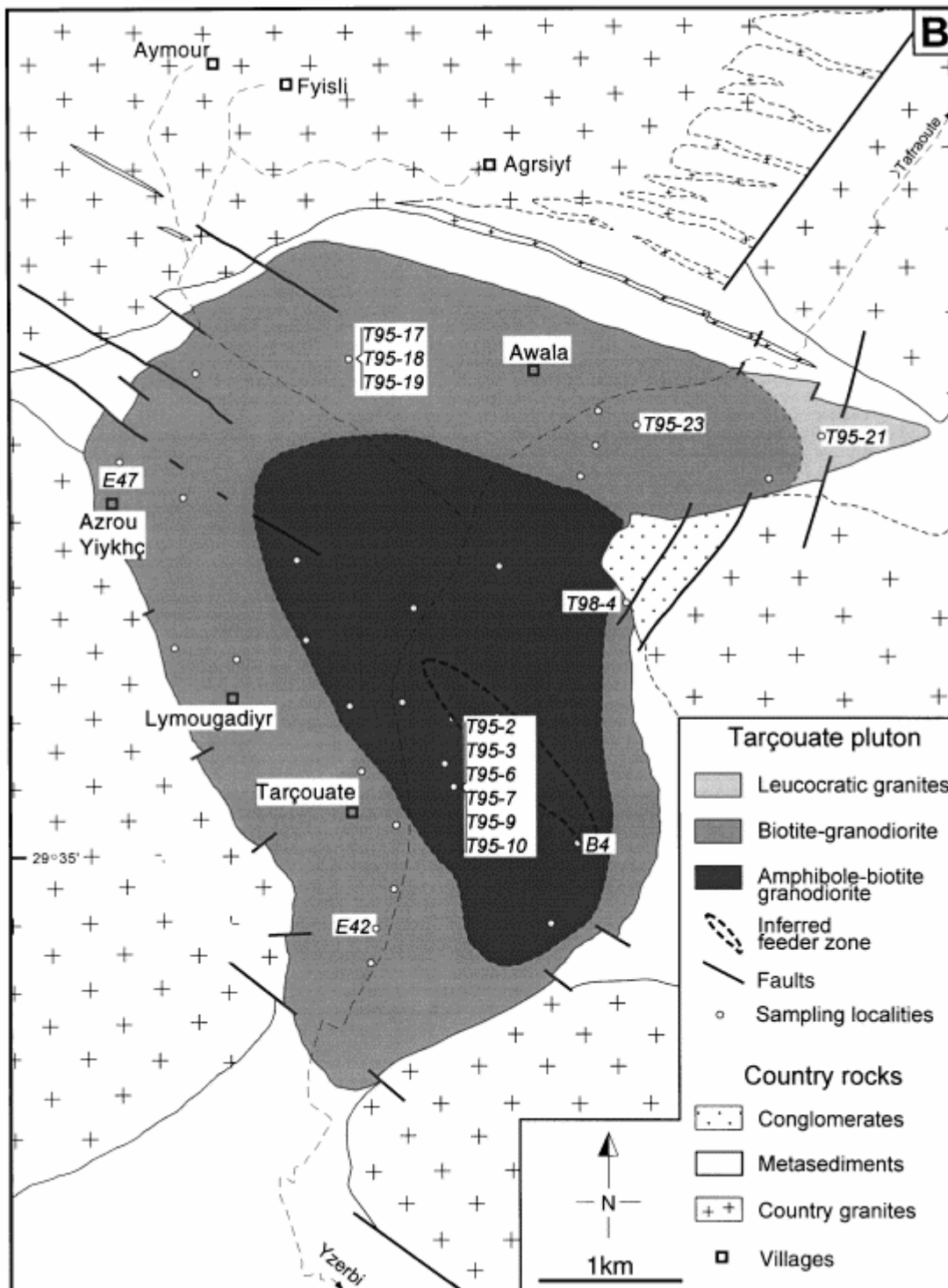


Fig. 1. Geological sketch maps of the Kerdous inlier (A) and of the Tarçouate pluton (B); modified from Choubert (1963). In (A) the Tahala pluton is Palaeoproterozoic, whereas the Tarçouate and Tafraoute plutons are Neoproterozoic in age.

3. Lithology and mineral compositions

The Tarçouate pluton is a zoned laccolith-shaped intrusion, 5 km in diameter, with an irregular outline (Fig. 1B). It consists of the following lithological units:

(1) A main unit consists of hornblende- and biotite-bearing granodiorites (hereafter referred to as hbl–granodiorites) and aplite dykes in its centre, and of hornblende-free biotite-bearing granodiorites (bt–granodiorites) in its periphery. The contact between the two types of granodiorites, as far as it can be seen, appears to be sharp but lobate, and is seemingly of syn-magmatic nature. Monzodiorites occur as decimetre-sized microgranular enclaves scattered throughout the pluton, and as swarms of large enclaves restricted to the pluton centre and corresponding to more or less fragmented syn-plutonic dykes cutting across the hbl–granodiorites. Field relationships show that all these lithologies emplaced in a short time span, before granodiorites crossed the granite solidus. No country schist enclaves were observed in any of these lithologies.

(2) A subordinate outer unit consists of muscovite-bearing leucocratic to hololeucocratic granites and pegmatites (hereafter referred to as leucocratic granites), localised mainly to the northern edge of the pluton. These granites also occur as sills in the surrounding schists at the top of the pluton. They are free of monzodioritic microgranular enclaves, but may locally contain rare small schist enclaves.

Structural data (Nachit et al., 1999) show that the pluton is inversely zoned and was formed by the in situ assemblage and structuration of successive batches of less and less differentiated magmas supplied from a unique, off centre, feeder zone. The emplacement succession deduced from field relationships is as follows: leucocratic granites, bt–granodiorites (+monzodiorite enclaves), hbl–granodiorites (+monzodiorite enclaves), and monzodiorite syn-plutonic dykes. Strain in the central part of the pluton is typically low and displays a constrictional type of deformation, whereas flattening is predominant in the periphery and increases towards the pluton edges. The growth of the pluton (ballooning) resulted in a circumferential stretching lineation and an increase in flattening towards the periphery. This is especially visible towards the top of the pluton where the sills of leucocratic granites are deformed and folded in response to pluton inflation, corroborating that granites emplaced before granodiorites. This lateral spreading took place within the soft country schists, and was subsequently impeded by older resistant granitic bodies, leading to the irregular “amoeba-like” outline of the pluton (Fig. 1B).

We report here only on the main mineralogical features, which are then used to decipher the conditions of emplacement. Modal compositions are summarised in Table 1.

3.1. Granodiorites and leucocratic granites

Hbl–granodiorites are medium-grained porphyritic rocks, which display layered and homogeneous varieties. The layered ones display a rhythmic, mineral-graded, horizontal layering with common trough-banding and cross-stratifications. Aplite dykes, associated with the hbl–granodiorites in the pluton centre, are hornblende-free and biotite-bearing and also comprise homogeneous and layered varieties. In rare cases, veins of biotite-rocks cut across the hbl–granodiorites. The bt–granodiorites are commonly medium-grained, equigranular, homogeneous rocks, but may contain, locally, clusters of K-feldspar phenocrysts. The

leucocratic granites from the outer unit are medium-grained, equigranular, homogeneous rocks, which differ by the presence of muscovite (\pm biotite) and more sodic plagioclase.

Table 1. Modal compositions of the main rock types from the Tarçouate pluton (vol.%)

Hbl–granodiorites
Qtz (20–25), Kfs (5–25), Pl (40–50), Hbl (5–10), Bt (5–10)
Bt–granodiorites
Qtz (25–30), Kfs (20–25), Pl (40), Bt (10)
Leucocratic granites
Qtz (25–35), Kfs (20–35), Pl (30–40), Mu (5–10), Bt (0–2)
Monzodiorites
Qtz (1–10), Kfs (0–7), Pl (25–35), Hbl (0–35), Bt (5–45)

Mineral abbreviations according to Kretz (1983).

Plagioclase occurs as millimetre- to centimetre-sized anhedral to euhedral normally zoned crystals. The anorthite content decreases from hbl–granodiorites (An_{24-36}) to bt–granodiorites (An_{14-23}) and leucocratic granites (An_{2-15}). K-feldspar phenocrysts are heterogeneously distributed and a slight increase in their size is observed close to monzodioritic dykes. K-feldspar composition is richer in albite in the hbl–granodiorites (Or_{74-76}), than in the bt–granodiorites (Or_{94-96}), wherein perthites appear to be more abundant.

Amphibole is restricted to the granodiorites from the pluton centre, but occurs exceptionally in the periphery where monzodioritic enclaves are abundant (Azrou Yiykhç, Fig. 1B). Amphibole is associated with biotite as half-centimetre-sized clusters, or occurs as inclusions within feldspars. It corresponds to a ferro-edenite according to Leake et al. (1997), with $0.55 \leq X_{Fe} \leq 0.57$, $1.7 \leq Al_{tot} \leq 1.9$ and $0.13 \leq Ti \leq 0.24$ atom per formula unit (apfu). Biotite occurs generally as millimetre-sized aggregates of brown flakes with greenish rims. It can be locally retrogressed along cleavages into chlorite, rutile and prehnite. Biotite X_{Fe} ratios show an increase (Fig. 2) from the layered hbl–granodiorites ($X_{Fe}=0.54-0.59$) to the homogeneous hbl–granodiorites ($X_{Fe}=0.61-0.64$) and to the bt–granodiorites ($X_{Fe}=0.67-0.70$). However, Al_{tot} contents increase abruptly from the hbl–granodiorites ($Al_{tot}=2.70-2.94$ apfu) to the bt–granodiorites ($Al_{tot}=3.02-3.20$ apfu). These covariations indicate a difference in the peraluminosity of the parental magmas.

Accessories consist of allanite, pistachite, sphene, apatite, zircon and ilmenite in the hbl– and bt–granodiorites, and of zircon, sphene and magnetite in the leucocratic granites. Two types of epidote have been found: (i) magmatic epidote ($24 \leq Ps \leq 36$) appears as primary euhedral grains included in major phases (biotite or unaltered plagioclase) or concentrated in schlieren, and as epitaxial overgrowth on allanite; and (ii) secondary epidote consisting of anhedral to subhedral grains in sericitised plagioclase ($Ps \approx 25$) or in the cleavage of biotite ($34 \leq Ps \leq 36$). A morphological study of zircon from the hbl–granodiorites (Aït Malek, 1997) shows that it displays a simple concentric zoning, with rare inherited cores, and a habit similar to zircons from crustal granites according to the typology of Pupin (1980).

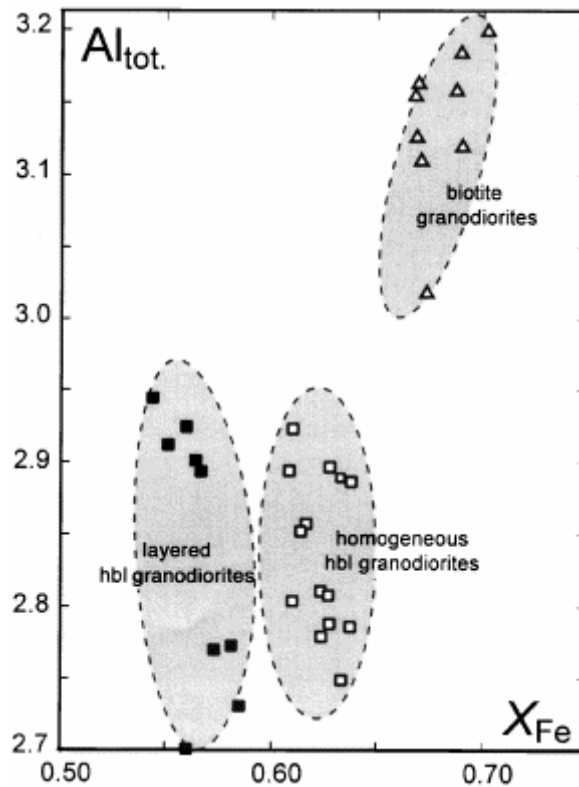


Fig. 2. Plot of Al_{tot} (atom per formula unit) vs. X_{Fe} for biotites from the hbl- and bt-granodiorites.

3.2. Monzodiorites

The bulk mineralogical composition of microgranular enclaves and syn-plutonic dykes averages that of monzodiorites and quartz-monzodiorites (Table 1), with amphibole-bearing (hbl=20–35%, BT=5–20%) and amphibole-free (bt=35–45%) varieties. Scattered monzodiorite enclaves are rather small (≤ 20 cm, especially in bt-granodiorites) and contain significant amounts of biotite, whereas in the centre of the main unit, monzodiorites occurring mainly as fragmented syn-plutonic dykes are dominantly hornblende-bearing. Some enclaves from the bt-granodiorites display a foliation outlined by the preferred orientation of biotite.

Xenocrystic quartz (commonly rimmed with amphibole), K-feldspar and plagioclase crystals are widespread, although in variable amounts. The sum of quartz and feldspars ranges from a few percents in the scattered enclaves to more than 30% in the dykes. Quartz also occurs as an interstitial phase. K-feldspar occurs as rounded megacrysts suggesting partial resorption, whereas plagioclase display three distinct morphologies: subhedral to euhedral laths with complex zonation (An_{25-55}), xenocrysts with patchy zoning (An_{22-28}), and anhedral interstitial grains associated with the ferromagnesian phases (An_{4-15}).

Amphibole occurs as subhedral to euhedral, locally skeletal crystals, and in a few cases, forms aggregates (former pyroxenes?). It has the composition of ferro- and magnesio-hornblende, tschermakite or hastingsite, and displays variable X_{Fe} values (0.53–0.67 in the scattered enclaves, 0.40–0.66 in the dykes). Biotite from the syn-plutonic dykes display a more restricted compositional range ($0.43 < X_{Fe} < 0.52$; $2.84 < Al_{tot} < 2.99$ apfu) than the scattered enclaves, which tend to be richer in iron ($0.44 < X_{Fe} < 0.64$) and in Al_{tot} (2.80–3.20 apfu).

Accessories comprise epidote, ilmenite, sphene, apatite and zircon. Epidote, preferentially found in the monzodiorite dykes, occurs as euhedral, probably magmatic crystals, or as a late-magmatic phase replacing hornblende (e.g. Zen and Hammarstrom, 1984) and plagioclase, or filling late crosscutting veins. Its composition ranges from Ps-26 (core) to Ps-32 (rim). Zircons are free from inherited cores and display the morphology of zircons from the calc-alkaline/sub-alkaline series in Pupin's typology (Aït Malek, 1997).

3.3. *P–T* conditions of emplacement

Temperatures have been estimated using zircon and apatite solubilities (Watson and Harrison) along with Ti-in-amphibole thermometry (Spear and Raase). Zircon and apatite thermometers were applied to the homogeneous hbl–granodiorites and to the bt–granodiorites, the layered granodiorites being excluded because of their cumulative character. Saturation temperatures estimated from the Zr contents are in the 745–805 °C range, whereas those calculated from the P₂O₅ contents are much higher (880–910 °C). This discrepancy may suggest that apatite is an early crystallising phase (see for instance Hoskin et al., 2000). The average Ti content of hornblendes from the granodiorites ($\bar{x}=0.18\pm0.04$ apfu), not significantly different from that of the monzodiorites ($\bar{x}=0.16\pm0.04$ apfu), yields an average temperature estimate of 760±50 °C. The temperature range estimated from thermometry is consistent with experimental data on the liquidus temperature of hornblende in granodiorites (<950 °C; Gilbert et al., 1982).

Pressure conditions were estimated from the Al-in-hornblende barometer using the calibration of Anderson and Smith (1995), which accounts for the temperature effect. The total Al content in the hbl–granodiorites ranges from 1.72 to 1.88 apfu ($\bar{x}=1.79\pm0.06$), therefore yielding 380<*P*<410 MPa, for the above *T* range (745–805 °C). These values are consistent with the presence of magmatic epidote, which seems to occur in plutons emplaced at *P*≥280 MPa (e.g. Vyhnal et al., 1991), but should be considered as an upper limit for the emplacement conditions because of the presence of widespread andalusite in the metapelites from the contact aureole. This discrepancy may either reflect problems inherent to the Al-in-hornblende barometer, or suggest that amphibole-melt equilibration may have occurred at levels deeper than that of emplacement.

4. Chemical and isotopic data

Although only representative major- and trace-element analyses are given in Table 2, all major- and trace-element data are presented in the chemical diagrams (Fig. 3, Fig. 4, Fig. 5, Fig. 6 and Fig. 7). The full set of data on mineral and whole-rock compositions is available on request. Sr and Nd isotopic data are given in Table 3 and Fig. 8. Accounting for the zircon U–Pb age published by Aït Malek et al. (1998), and for field data showing the synchronous emplacement of the different lithologies of the Tarçouate pluton, the ⁸⁷Sr/⁸⁶Sr initial ratios and ε_{Nd} values were calculated at 583 Ma.

Table 2. Representative major (wt.%) and trace (ppm) element compositions of granodiorites and related rocks from the Tarçouate pluton

Sample	Hornblende granodiorites		Biotite granodiorites		Aplite	Leucocratic outer unit		Granites sill	Monzodiorites		Scattered enclaves		Host metapelite
	95-9 ^a	95-7 ^b	95-19	E47	95-2	E42a	95-21	98-4 ^c	95-6	B4	95-18	95-17	98-8
SiO ₂	58.18	63.81	68.87	71.00	75.70	72.46	74.41	74.71	51.48	52.13	50.33	54.01	60.44
Al ₂ O ₃	16.43	16.92	15.58	15.95	12.88	14.04	13.92	15.14	19.62	19.53	19.04	16.93	20.13
Fe ₂ O ₃ ^d	8.42	4.35	2.85	2.45	0.76	2.59	1.49	0.96	8.66	8.58	11.28	8.88	7.63
MnO	0.09	0.05	0.04	0.03	— ^e	—	—	—	0.14	0.16	0.17	0.20	0.02
MgO	2.58	1.34	0.65	0.66	0.04	0.77	0.24	0.10	2.88	2.62	3.17	4.38	1.84
CaO	4.50	3.87	2.46	1.88	0.86	0.81	0.56	0.55	7.10	7.87	3.60	6.03	0.51
Na ₂ O	4.02	4.59	4.51	3.74	3.54	4.26	3.77	4.70	5.21	5.38	4.66	3.93	1.01
K ₂ O	2.93	2.95	3.59	3.77	5.31	3.05	4.04	2.43	1.79	1.08	4.05	2.65	4.58
TiO ₂	1.23	0.60	0.35	0.31	0.03	0.27	0.12	—	1.52	0.84	1.31	1.24	0.63
P ₂ O ₅	0.43	0.25	0.14	0.09	0.03	0.08	0.11	0.22	0.33	0.40	0.46	0.24	0.15
L.O.I. ^f	0.80	0.84	0.55	0.50	0.64	1.30	1.07	0.94	0.95	1.18	1.65	1.26	2.97
Total	99.61	99.57	99.59	100.38	99.79	99.63	99.73	99.75	99.68	99.77	99.72	99.75	99.92
Rb	126	90	102		118	113	128	148	64	25	282	139	195
Sr	504	570	386	331	89	216	109	40	668	628	322	392	115
Ba	1467	1652	1496	1176	125	1439	818	16	604	316	606	354	721
Cr	20	10	10		2	60	6		9	5	74	40	131
Zn	119	59	55	41	9	24	11	29	109	102	208	155	102
Zr	239	151	122	148	50	86	109	33	101	158	174	106	141
Y	12	7	8	11	0.8	32	24	5	14	33	17	17	25
La	57.3	31.1	25.8	30.1	5.5	30.4	52.2	1.8	20.7	25.3	15.0	18.4	31.5
Ce	103.9	55.5	49.4	65.2	7.6	58.5	128.4	3.2	51.9	62.8	22.8	36.9	63.2
Pr	12.8	6.2	5.2		0.7	6.5	13.9	0.4	7.2	9.2	3.8	5.0	7.8
Nd	45.9	23.4	20.7		1.7	24.0	56.6	1.8	31.9	41.6	19.8	22.4	30.0
Sm	6.8	4.0	3.8	4.2	0.2	5.1	10.6	0.5	6.1	10.2	5.9	4.9	5.8
Eu	1.8	1.4	1.1	1.1	0.1	1.1	1.2	0.06	3.0	2.4	1.0	1.9	1.3
Gd	5.0	3.1	2.5		0.2	4.1	6.7	0.4	4.8	8.0	4.6	4.1	5.0
Tb	0.6	0.4	0.3		0.02	0.8	0.9	0.1	0.6	1.2	0.7	0.6	0.8
Dy	2.7	1.6	1.6	2.3	0.1	4.9	4.4	0.6	2.8	6.0	3.3	2.9	4.2
Ho	0.4	0.3	0.3		0.03	1.2	0.9	0.1	0.5	1.2	0.7	0.6	0.8
Er	1.0	0.6	0.7		0.07	3.1	2.2	0.4	1.0	2.9	1.4	1.6	2.3
Tm	0.1	0.1	0.1		0.02	0.5	0.3	0.06	0.2	0.4	0.2	0.2	0.3
Yb	0.8	0.5	0.6	0.9	0.1	2.8	1.8	0.6	1.1	2.6	1.0	1.4	2.3
Lu	0.1	0.1	0.1		0.02	0.4	0.2	0.1	0.2	0.4	0.1	0.2	0.4

Analytical methods: Major and trace elements determined by ICP-AES and ICP-MS (CRPG-CNRS, Nancy). Analytical uncertainties are estimated at 2% for major elements, and at 5% or 10% for trace-element concentrations (except REE) higher or lower than 20 ppm, respectively. Precision for REE is estimated at 5% when chondrite-normalized concentrations are >10 and at 10% when they are lower.

Table 3. Sr and Nd isotopic compositions of granodiorites and related rocks from the Tarçouate pluton

	Sample	Rb	Sr	⁸⁷ Rb/ ⁸⁶ Sr	⁸⁷ Sr/ ⁸⁶ Sr	⁸⁷ Sr/ ⁸⁶ Sr _{t=583}	Sm	Nd	¹⁴⁷ Sm/ ¹⁴⁴ Nd	¹⁴³ Nd/ ¹⁴⁴ Nd	εNd _{t=583}
<i>Hbl – granodiorites and related rocks (main unit)</i>											
Granodiorite	95-7	89.7	569.7	0.4555	0.710983 ± 27	0.70720	3.93	22.44	0.10601	0.512208 ± 25	– 1.66
Granodiorite	95-10	76.7	569.0	0.3904	0.710528 ± 15	0.70728	3.87	20.22	0.10810	0.512209 ± 12	– 1.80
Aplite	95-3	117.1	198.0	1.6850	0.720748 ± 26	0.70674	0.40	2.89	0.08359	0.512088 ± 62	– 2.33
Monzodiorite ^a	95-6	63.8	668.1	0.2763	0.709490 ± 26	0.70719	6.31	29.96	0.12742	0.512337 ± 7	– 0.74
<i>Bt – granodiorites and related enclaves (main unit)</i>											
Granodiorite	95-19	101.9	386.1	0.7644	0.714270 ± 35	0.70792	3.45	18.53	0.11248	0.512194 ± 8	– 2.42
Granodiorite	95-23	89.8	418.6	0.6211	0.713174 ± 26	0.70801	4.62	28.30	0.09761	0.512118 ± 10	– 2.79
Monzodiorite ^b	95-17	139.1	391.5	1.0288	0.716781 ± 38	0.70823	4.93	21.99	0.13550	0.512304 ± 11	– 1.99
Monzodiorite ^c	95-18	281.8	321.7	2.5377	0.724475 ± 40	0.70338	5.58	18.62	0.18129	0.512445 ± 11	– 2.65
<i>Leucocratic granites (outer unit)</i>											
Ms–granite	95-21	128.1	108.9	3.4271	0.776514 ± 18	0.74802	8.90	46.57	0.11549	0.511722 ± 9	– 11.86
Ms–pegmatite	98-4	132.0	40.5	9.6188	1.005477 ± 23	0.92552	0.48	1.73	0.16853	0.512118 ± 49	– 8.09
<i>Country rocks</i>											
Metapelite	98-8	195.0	115.1	4.9664	0.823047 ± 44	0.78176	6.06	31.7	0.11549	0.511592 ± 21	– 14.40

Analytical method: Rb–Sr and Sm–Nd separation techniques following Michard et al. (1985) and Boher et al. (1992). Rb, Sr, Sm and Nd determined using the isotope dilution method; Sr and Nd isotopic ratios measured using a Finnigan MAT 262 mass spectrometer. Chemistry blanks are of about 0.8 ng Sr for the acid dissolution and 2 ng Nd for the metaborate flux method. ⁸⁷Sr/⁸⁶Sr and ¹⁴³Nd/¹⁴⁴Nd ratios normalized to 0.1194 and 0.7219, respectively. Errors on ⁸⁷Rb/⁸⁶Sr and ¹⁴⁷Sm/¹⁴⁴Nd ratios estimated at 1.5% and 0.5%, respectively (2σ). Analytical errors on isotopic ratios are expressed as 2σ.

4.1. Major and trace elements in the granodiorites and leucocratic granites

The chondrite-normalised REE concentrations of both the hbl- and bt-granodiorites are indistinguishable (Fig. 3a,b). The patterns are strongly fractionated, with high chondrite-normalised La/Yb ratios ranging from 16 to 61 in the hbl-granodiorites and from 15 to 57 in the bt-granodiorites. The LREE contents are rather high ($73 < La_N < 235$), exceeding almost 200 times chondrite in layered hbl-granodiorites containing abundant accessories, whereas Yb contents are remarkably low ($2.5 < Yb_N < 6.8$, $\bar{x}=4.5$). The patterns have generally a positive Eu anomaly ($Eu/Eu^* \leq 1.4$), except for a few samples ($Eu/Eu^* \geq 0.87$). Aplite dykes have $(La/Yb)_N$ ratios (28–44) in the same range as the granodiorites, but differ by lower REE concentrations ($22 < La_N < 68$; $0.7 < Yb_N < 1.8$) consistent with their strongly differentiated nature. Leucocratic granites (Fig. 3c) display less fractionated patterns [$2 < (La/Yb)_N < 19$], much higher Yb contents ($11 < Yb_N < 18$, $\bar{x}=15$) and more negative Eu anomalies ($0.35 < Eu/Eu^* < 0.75$). These features are close to those of the surrounding schists (Fig. 3b), which closely match the North American Shale composite (Haskin et al., 1968). Pegmatitic granite from a sill at the top of the pluton (sample 98-4, Table 2) displays very low REE concentrations and a weakly fractionated pattern [$\Sigma REE=10.2$ ppm, $(La/Yb)_N=2.2$].

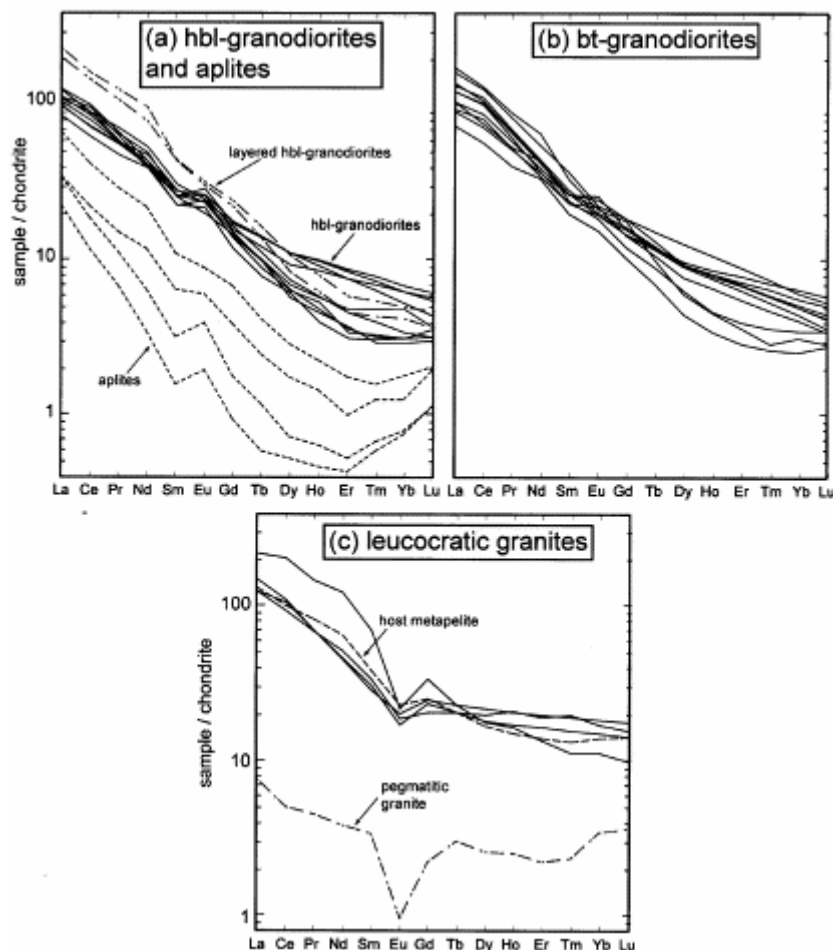


Fig. 3. Chondrite-normalized REE patterns for the (a) hbl-granodiorites and aplites, (b) bt-granodiorites and (c) leucocratic granites and country metapelite. Chondrite-normalisation factors from Evensen et al. (1978).

Other trace- and major element contents further show that the two types of granodiorite and the aplites form a chemically coherent entity. Y contents remain very low (5–12 ppm) in the granodiorites, whereas leucocratic granites display higher and more variable Y contents (24–88 ppm). The granodiorites and leucocratic granites are also distinguishable by their average Ba, Sr and CaO contents (Ba=1352 vs. 1030 ppm; Sr=423 vs. 144 ppm; Ca=2.77% vs. 1.05%). The $\text{Al}_2\text{O}_3/(\text{CaO}+\text{Na}_2\text{O}+\text{K}_2\text{O})$ molecular ratios (Fig. 4) show that the hbl- and bt-granodiorites are metaluminous to peraluminous ($\bar{x}=1.00\pm 0.08$ and 1.12 ± 0.09 , respectively), whereas the leucocratic granites are distinctly peraluminous ($\bar{x}=1.20\pm 0.10$). These granites display high Na_2O contents (2.50–4.26%) and variable $\text{K}_2\text{O}/\text{Na}_2\text{O}$ ratios (0.72–1.94). The pegmatitic granite from a sill at the top of the pluton displays a low $\text{K}_2\text{O}/\text{Na}_2\text{O}$ ratio (0.52) and low Sr (40 ppm) and Zr (33 ppm) contents.

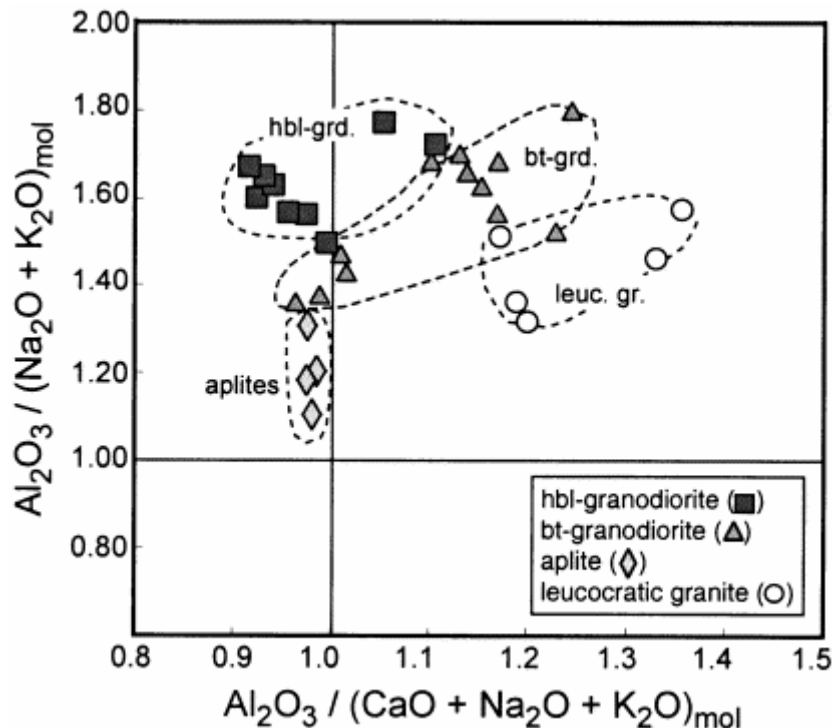


Fig. 4. A/NK vs. A/CNK diagram for the granodiorites and related rocks from the Tarçouate pluton.

In two-element variation diagrams (e.g. Fig. 5), hbl-granodiorites, bt-granodiorites and aplites (main unit) fall on a common differentiation trend, with SiO_2 contents increasing from the layered hbl-granodiorites (57–59%) to the homogeneous hbl-granodiorites (63–67%), and to the bt-granodiorites (67–72%) and aplites (70–76%). The leucocratic granites (outer unit) form a distinct trend which appears clearly, for example, on a Sr vs. CaO plot (Fig. 5a). All the data consistently show the presence of two distinct magmatic units in the Tarçouate pluton: one consisting of a differentiated metaluminous to slightly peraluminous granodiorite suite (I-type), and the other corresponding to peraluminous granites (S-type).

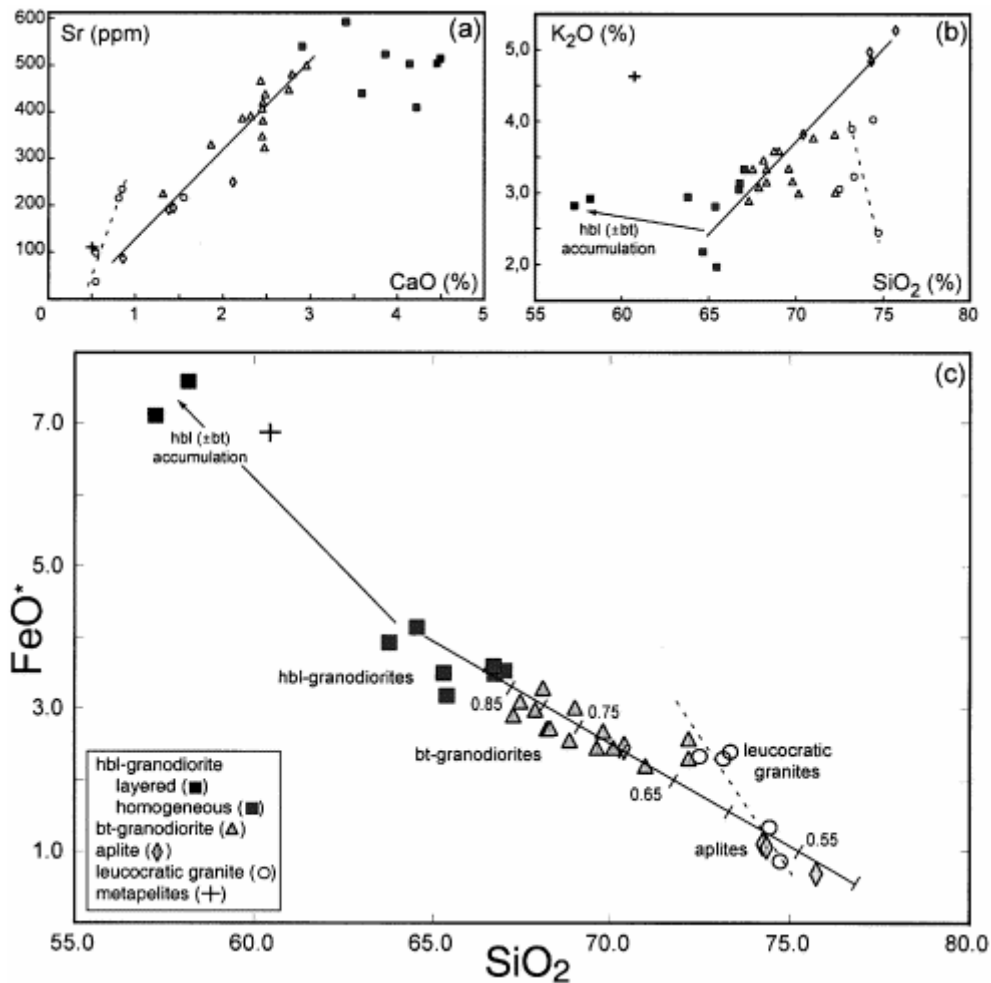


Fig. 5. Two-elements variation diagrams for the hbl- and bt-granodiorites, aplites, and leucocratic granites: (a) Sr–CaO, (b) K₂O–SiO₂ and (c) FeO*–SiO₂ (total iron as Fe²⁺). For the FeO*–SiO₂ plot, the solid line corresponds to the trend followed by a granodioritic magma (sample 95-7, Table 2) differentiated by fractional crystallisation involving pl_{An40}/hbl/bt/Fe–Ti–ox in the proportions 70.5:12.5:15:2 (numbered TICKMARKS=mass fraction of residual melt).

4.2. Major and trace elements in the monzodiorites

Scattered enclaves and syn-plutonic dykes (Fig. 6) display similar, moderately fractionated, REE patterns [$3.4 \leq (La/Yb)_N \leq 16.0$], although Eu anomalies are preferentially positive for the dykes ($0.8 \leq Eu/Eu^* \leq 1.7$) and negative for the enclaves ($0.4 \leq Eu/Eu^* \leq 0.7$, two values > 1.1 , excepted). Monzodiorites differ from the associated granodiorites by a more ferromagnesian chemistry ($Fe_2O_3 + MgO = 10.1–17.1\%$ vs. $3.1–10.7\%$) and higher CaO ($3.0–8.6\%$ vs. $1.3–4.5\%$), TiO₂ ($1.0–2.0\%$ vs. $0.3–1.2\%$) and HREE ($Yb_N = 6.8–15.6$ vs. $2.9–6.8$) contents. Foliated enclaves from the bt-granodiorites have the highest K₂O, total Fe₂O₃ and Rb contents (highest biotite content), whereas K₂O ($1.1–2.5\%$) and Rb ($25–88$ ppm) contents in the syn-plutonic dykes display a gradual increase up to the values observed in the hbl-granodiorites (K₂O = $2.0–3.3$, Rb = $79–126$). In major- and trace-element variation diagrams (Fig. 7), the two types of monzodiorite display distinct compositional trends with a control mainly by biotite in microgranular enclaves and by hornblende or the granodiorites (mingling?) in the syn-plutonic dykes.

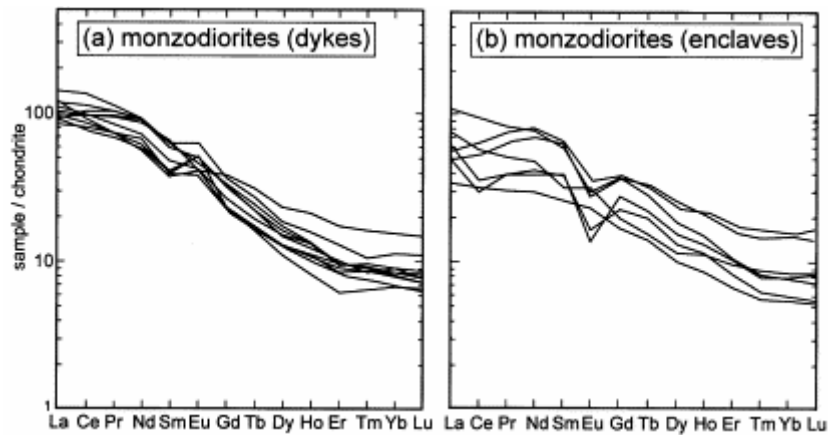


Fig. 6. Chondrite-normalized REE patterns for the monzodioritic microgranular enclaves and syn-plutonic dykes.

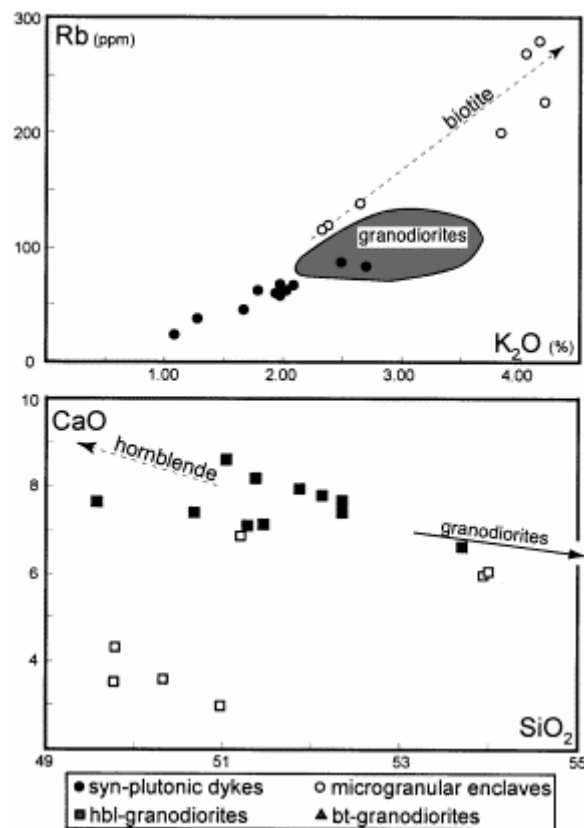


Fig. 7. Rb–K₂O and CaO–SiO₂ plots for the monzodiorites showing that the microgranular enclaves and syn-plutonic dykes form two distinct evolution trends. Field of hbl- and bt-granodiorite shown for comparison

4.3. Rb–Sr and Sm–Nd isotopic data

The three granite lithologies display $^{87}\text{Sr}/^{86}\text{Sr}$ initial ratios increasing from the hbl-granodiorites (0.7072–0.7073) to the bt-granodiorites (0.7079–0.7080) and the leucocratic granites (0.7480). However, the muscovite-bearing pegmatite sample (sample 98-4) shows an anomalously high $^{87}\text{Sr}/^{86}\text{Sr}$ initial ratio, suggesting subsequent perturbation of the Rb–Sr isotopic system and illustrating the problem of the Sr mobility in such rock types. Our data are consistent with the range in isotopic compositions previously published by Charlot (1982) for the granodiorites ($\text{Sr}_i=0.7073\text{--}0.7081$). Unfortunately, Charlot's data cannot be compared in

detail with ours because lithologies are not specified. Accounting for the 2σ errors on the $^{87}\text{Sr}/^{86}\text{Sr}$ data and for the $^{87}\text{Rb}/^{86}\text{Sr}$ values, the difference in isotopic ratios between the hbl- and bt-granodiorites can be considered as significant. In agreement with the Sr isotopic data, the three granite lithologies present different Nd isotopic compositions (Fig. 8). The ϵ_{Nd} values decrease from the hbl-granodiorites (-1.7 and -1.8) to the bt-granodiorites (-2.4 and -2.8) and to the leucocratic granites (-11.9). The $^{87}\text{Sr}/^{86}\text{Sr}$ initial ratio for aplite (0.7067) is not significantly different from that of the hbl-granodiorites, whereas the ϵ_{Nd} value (-2.3) is closer to that of the bt-granodiorites. It must be emphasized that the aplite dykes and hbl-granodiorites are associated in the centre of the pluton.

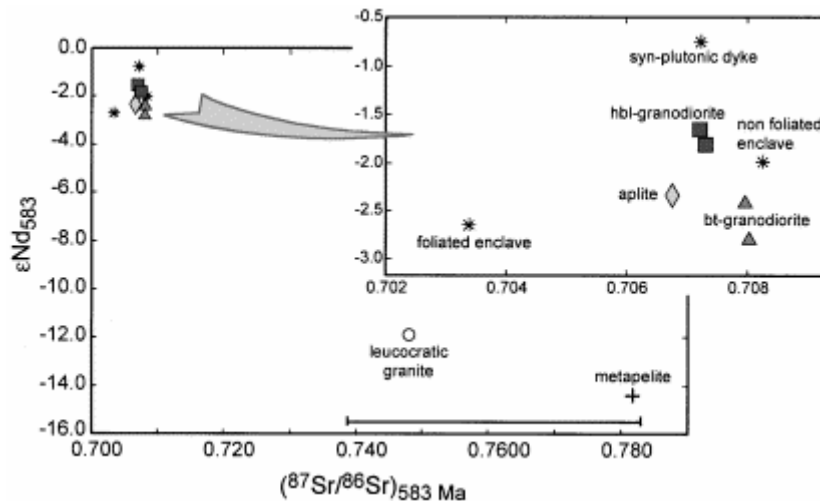


Fig. 8. ϵ_{Nd} vs. $^{87}\text{Sr}/^{86}\text{Sr}$ at 583 Ma for granodiorites and related rocks from the Tarçouate pluton. Horizontal BAR=range in $^{87}\text{Sr}/^{86}\text{Sr}$ initial ratios of the country metasediments (Charlot, 1982).

Some monzodiorites display $^{87}\text{Sr}/^{86}\text{Sr}$ initial ratios closely similar to those of their host granodiorites: 0.7072 for a monzodiorite from a syn-plutonic dyke vs. 0.7072 for its host hbl-granodiorite, 0.7082 vs. 0.7079 for a nonfoliated monzodiorite enclave and its host bt-granodiorite (Table 3). However, the strongly foliated enclave collected in the bt-granodiorite displays an anomalously low $^{87}\text{Sr}/^{86}\text{Sr}$ isotopic initial ratio (0.7034). The Nd isotopic compositions are more heterogeneous with ϵ_{Nd} values higher in the monzodiorites than in their host granodiorites (-0.7 vs. -1.6 and -2.0 vs. -2.4), with the exception of the foliated enclave. The monzodiorite from a syn-plutonic dyke is distinguishable by a less negative ϵ_{Nd} value (-0.7) compared with those of the microgranular enclaves (-2.0 and -2.7).

5. Discussion

5.1. Genesis of the granodiorites and leucocratic granites

Isotopic data, major- and trace-element compositions and petrogenetic modelling allow the genetic relationships between the hbl-granodiorites, bt-granodiorites and aplites to be discussed. We suggest that they were derived from a common HREE-poor parental magma by whole-rock assimilation and fractional crystallisation (AFC):

(1) Plot of the major- and trace-element data along a single evolution trend on two-element variation diagrams, together with the close similarity of the REE patterns of both types of granodiorites (especially the low HREE contents), are consistent with their differentiation by

fractional crystallisation from a common parent. However, the absence of correlation between differentiation indices (e.g. SiO_2) and some trace elements (e.g. REE), along with the presence of layered and schlieren granodiorites, suggest that fractionation trends may have been partly blurred by accumulation processes. Increase of biotite X_{Fe} ratio and decrease of plagioclase An content from the hbl–granodiorites to the bt–granodiorites are also consistent with fractional crystallisation. The distinct isotopic compositions and biotite Al_{tot} contents show, however, that the hbl–granodiorites, bt–granodiorites and aplites cannot be derived simply by closed-system fractional crystallisation but also involved wallrock assimilation. The strong increase of biotite Al_{tot} contents, along with the concomitant increase in whole-rock $^{87}\text{Sr}/^{86}\text{Sr}$ initial ratios and decrease in the ϵ_{Nd} values from the hbl–granodiorites to the bt–granodiorites, suggest the incorporation of peraluminous crustal material (more radiogenic Sr and higher A/CNK ratios).

(2) The fractionated, LREE-rich and HREE-poor patterns of the hbl– and bt–granodiorites suggest that their parent magma was in equilibrium with a hornblende–garnet-bearing residue, and that the source was enriched in LREE. The patterns resemble those of high-K calc-alkaline monzonitic suites assumed to have formed by partial melting of amphibole- and garnet-bearing mafic rocks (e.g. Martin and Rapela). Moderate amount of partial melting ($F=0.17$) of a LILE-enriched tholeiite parent, leaving a garnet-bearing residue (hbl/pl/grt/cpx/ilm=51:29.5:10:7.5:2 wt.%), can account for the composition of the less differentiated granodiorite (sample 95-7, Table 2). Nevertheless, the rather high initial ratios of the hbl–granodiorites and the occurrence of associated mafic microgranular enclaves suggest that they originate from an hybridised parental magma (e.g. Dias and Leterrier, 1994). The high $^{87}\text{Sr}/^{86}\text{Sr}$ initial ratio (0.7480) of the leucocratic granites, which is within the range of initial ratios of the surrounding metasediments ($0.7393 < ^{87}\text{Sr}/^{86}\text{Sr}_i < 0.7819$; Charlot, 1982), and their low ϵ_{Nd} values (-8.1 and -11.9) comparable to that of the analyzed metapelite ($\epsilon_{\text{Nd}} = -14.4$), suggest an origin by partial melting from the country metasediments. However, the lower $\text{FeO}^*/\text{SiO}_2$ (Fig. 5c) and higher Na/Ca and Na/K ratios of these granites compared to those of the surrounding metapelites, suggest that the leucocratic granites cannot be derived by partial melting of the sole metapelites, but implies a more heterogeneous and immature sedimentary source (metagreywackes).

(3) Major-element modelling using a simple mass balance equation linking the composition of the initial melt to the amount and composition of the residual melt fraction and of the solid residue (Fig. 5c and Table 4) shows that the hbl– and bt–granodiorites can be derived by fractional crystallisation of a common parent melt with the composition of the less differentiated homogeneous hbl–granodiorites (i.e. sample 95-7, Table 2), leaving a residue composed of plagioclase/hornblende/biotite/oxides in the proportion 70.5:12.5:15:2 wt.% for $F=0.75$ ($\Sigma r^2=0.33$). The whole compositional range of granodiorites can be accounted for by residual melt fractions $F > 0.85$ for the hbl–granodiorites, $0.85 < F < 0.65$ for the bt–granodiorites, and $0.70 < F < 0.53$ for aplites (Fig. 5c). AFC modelling was performed using Sr and Nd isotopic data and DePaolo's (1981) equation (Table 4). The nature of the contaminant can reasonably be assumed to correspond to either the metasediments or the leucocratic granite melts. In the first case, we consider that contamination is due to the assimilation of both the melt and the residue; in the second case, of the melt only. Choosing metasediments or leucocratic granites as contaminant does not basically change AFC modelling because (i) the leucocratic granites are likely to derive from melting of the metasediments, and (ii) the Sr isotopic composition of these granites are within that of the metasediments. Modelling suggests limited amount of contamination for generating the bt–granodiorites, with r ratios (mass of material assimilated to the mass of material crystallized) ranging from 0.17 to 0.20

depending on the contaminant (metapelite or leucocratic granite, respectively), for $F=0.75$. This corresponds to an assimilation of ~ 5 wt.% of crustal material. Lastly, the Nd isotopic composition of the aplite sample is also consistent with its derivation from the hbl–granodioritic magma, but with a very low amount of contamination ($r=0.05$ for $F=0.55$, i.e. ~ 2 wt.% of wallrock assimilation) irrespective of the nature of the contaminant.

Table 4. Results of petrogenetic modelling compared with a representative bt–granodiorite composition. The bt–granodiorites are assumed to be derived from the less differentiated hbl–granodiorites by fractional crystallisation involving assimilation of metasediments.

	Solid residue							Modelled melt ($F = 0.75$)	Biotite granodiorite (95-23)
	Hbl	Pl	Kfs	Bt	Ilm	Ti-mt	Bulk		
<i>Major elements</i>									
SiO ₂	44.5	58.5	64.3	38.1			52.5	69.3	69.5
Al ₂ O ₃	10.3	26.4	19.2	16.3			22.3	15.6	15.9
FeO	20.3	0.0	0.0	25.0	50	80	7.6	2.8	2.8
MgO	8.9	0.0	0.0	8.4			2.4	1.1	0.9
CaO	12.0	8.0	0.4	0.0			7.1	2.8	2.5
Na ₂ O	1.3	7.1	3.2	0.0			5.2	4.5	4.6
K ₂ O	1.1	0.0	12.9	10.0			1.6	3.5	3.4
TiO ₂	1.6	0.0	0.0	2.2	50	20	1.2	0.4	0.4
<i>Trace elements and isotopes (AFC)</i>									
Sr								303	419
Nd								26	28
(⁸⁷ Sr/ ⁸⁶ Sr) _t								0.70800	0.70801
(¹⁴³ Nd/ ¹⁴⁴ Nd) _t								0.51175	0.51175

Major element modelling. Parent magma: sample 95-7 (Table 2). Modal composition of the residue: hbl/pl/bt/Fe–Ti–ox=12.5:70.5:15:2 (wt.%). Mass balance equation: $C_0 = FC_1 + (1-F)C_r$ where C_0 , C_1 and C_r are the compositions of the initial melt, of the residual melt and of the solid residue. AFC modelling. Parent melt: sample 95-7 (Table 3); contaminant: metapelite 98-8 (Table 3); $r=0.17$; Sr and Nd partition coefficients for hbl/pl/bt are 0.02:3.5:0.12 and 4.2:0.2:0.04, respectively (data from Arth and Hanson, 1975, with the exception of the Sr partition coefficient for plagioclase from Blundy and Wood, 1991). Eq. (15b) from DePaolo (1981).

5.2. Mafic microgranular enclaves and syn-plutonic dykes

The mafic microgranular enclaves and the syn-plutonic dykes display distinct major, trace and isotopic (Nd) compositions. The syn-plutonic dykes appear to be less differentiated (more Mg-rich hornblende and biotite, hornblende as the dominant ferromagnesian phase) and less contaminated than the scattered smaller microgranular enclaves (less Mg-rich biotite as the dominant phase), and both rock types display distinct chemical evolution trends. This may reflect either distinct parental magmas (e.g. Dias and Veloso), or different mechanisms or degrees of interaction of the mafic magma with the partially crystallised host–granodiorites, or both. This, along with their distinct occurrences, suggest that they correspond to several pulses of mafic magmas, as already reported in similar plutonic environments (e.g. Wiebe, 1994). The lower contamination of the syn-plutonic dykes could reflect weaker interactions with the hbl–granodiorites, whereas the higher contamination of the microgranular enclaves and their occurrence as small bodies could suggest a higher degree of interaction (stronger fragmentation, diffusion of water and alkalis, etc.). However, it must be noted that this remains speculative because the composition of the parental mafic magma is not known.

The homogeneity of Sr isotopic compositions between granodiorites, some monzodioritic enclaves, and the aplite dyke as well, suggests re-equilibration with the host rocks as shown by the distinct Nd isotopic initial ratios (see for instance Ben; Holden; Gasquet and Dias).

5.3. Differentiation, emplacement and magma–host interactions

Chemical and isotopic compositions show that the hbl– and bt–granodiorites are likely to arise from the differentiation of a common parental magma by fractional crystallisation, combined with assimilation of an alumina-rich crustal component. Moreover, emplacement of peraluminous granites with a crustal signature shows that significant amounts of anatectic melts were generated coevally. Several arguments show that the differentiation of the bt–granodiorites did not occur at the level of emplacement and consolidation, but at deeper levels in the crust:

- (1) Field relationships show an inverse zonation resulting from the aggregation of four main magma pulses, successively: leucocratic granites, bt–granodiorites (\pm monzodiorites), hbl–granodiorites (\pm monzodiorites) and monzodioritic dykes.
- (2) The higher proportions (about three times in volume) of bt–granodiorites with respect to the hbl–granodiorites is inconsistent with in situ differentiation.
- (3) The low biotite Al_{tot} content of the layered hbl–granodiorites (compared to that of the hbl– and bt–granodiorites) suggests that these rocks cannot correspond to the cumulates resulting from the differentiation of the bt–granodiorites by AFC. These cumulates should have been stored deeper into the crust.
- (4) The rarity of migmatites in the contact aureole suggests minor interaction between the granodioritic magmas and the country rocks.

Differentiation of the hbl–granodioritic magma at the level of consolidation is attested by the presence of a widespread rhythmic layering in the hbl–granodiorites, with alternating quartzofeldspathic and ferromagnesian mineral-graded layers, trough-banding and cross-layering. This suggests that the core of the pluton, consisting of a metaluminous crystal-poor granodioritic magma, behaved as a convecting magma chamber (e.g. Wiebe and Collins, 1998). Preservation of the isotopic heterogeneities of granodiorites, the lack of country schist enclaves in the granodiorites, and the rarity of migmatites in the contact aureole, all indicate that contamination at the level of emplacement is likely to have been low. However, two observations show that there was probably contamination with the country rocks at the level of emplacement during the differentiation of the hbl–granodiorites:

- (1) The biotites in both the layered and homogeneous hbl–granodiorites display scattered Al_{tot} contents at rather constant X_{Fe} values (Fig. 2). This could suggest that biotites may have equilibrated with chemically heterogeneous magmas with variable A/CNK ratios (a few hbl–granodiorites are distinctly peraluminous; Fig. 4), and therefore reflect either aggregation of chemically heterogeneous magma batches or variable contamination by the country rocks during differentiation.
- (2) The aplite dykes are closely related to the hbl–granodiorites (they are lacking in the bt–granodiorites) and show a clear chemical similarity with their host rocks (A/CNK ratios, REE patterns). However, the aplite analyzed displays a lower ϵ_{Nd} value than its host granodiorite.

This may suggest little contamination with the country rocks (~ 2 wt.% as suggested by AFC modelling) during differentiation of the granodioritic magma at the emplacement level, leading to residual melts with lower ϵ_{Nd} values.

The bt–granodiorites are homogeneous rocks that do not show any evidence of differentiation at the level of emplacement. The reasons for the lack of any layered structures are not clear, because the physical properties of the parent magma of the bt–granodiorites were probably not significantly different from that of the hbl–granodiorites, magmas having initial viscosities around $10^{4.5}$ Pa s (Scaillet et al., 1998). There might be interactions between the bt–granodiorites and the country schists, but as suggested by the absence of schist enclaves in the bt–granodiorites, by the rarity of migmatites in the contact aureole, and by the low degree of contamination with respect to the parent hbl–granodiorites, they were probably of very limited extent (in any case undetectable).

6. Conclusions

The following three points can be emphasized:

(1) The Tarçouate pluton is a shallow-level laccolith emplaced at 583 Ma, which results from the aggregation of different types of coeval magma batches (ranging from metaluminous to peraluminous in composition), forming an inverse succession: leucocratic granites, bt–granodiorites (\pm monzodioritic microgranular enclaves), hbl–granodiorites (\pm monzodioritic microgranular enclaves) and monzodioritic syn-plutonic dykes.

(2) Magma–host interactions are closely related to the differentiation and occurred at different levels. The parental magma of the bt–granodiorites formed at levels deeper than the level of consolidation, by fractional crystallisation of magmas similar in composition to the less differentiated hbl–granodiorites, with limited amounts (~ 5 wt.%) of contamination by a peraluminous crustal melt (\pm refractory residue?). The hbl–granodiorites differentiated at the level of consolidation by fractional crystallisation (igneous layering), involving small amounts of contamination (~ 2 wt.%) by the country rocks, which led to slightly contaminated residual melts (aplites). Therefore, contamination occurred dominantly before emplacement and remained limited at the consolidation level.

(3) These data preclude any significant material transfer process (see Paterson et al., 1996; their Fig. 8) for the emplacement of the Tarçouate pluton, but rather suggest an assembly of successive pulses of variably differentiated magmas. This is in close agreement with the statement of Pitcher (1979) that plutons are “constructed by multiple injection of magmas which differentiated elsewhere”. This, along with evidence of in situ differentiation of the hbl–granodiorites in a convecting chamber (igneous layering), and emplacement of monzodiorites as syn-plutonic dykes, implies that the pluton was built up from crystal-poor melts transferred through dykes by pulses (e.g. Vigneresse and Clemens, 2000). Furthermore, as dyke ascent of granitic magma is probably rapid enough to preclude significant interactions with wallrocks (Clemens and Mawer, 1992), it is likely that differentiation and interaction with the country rocks dominantly occurred deeper in the crust in an intermediate chamber. These pulses accumulated by lateral spreading along rheological discontinuities and upheaval of the schist cover (Hogan and Vigneresse). These shallow level granitic plutons can be considered as an end-member of magma emplacement with minimum interactions with the country rocks.

Acknowledgements

We are indebted to L. Reisberg, F. Vidal and H. Martin for providing us with isotopic data. Thanks to J.P. Burg, D. Gasquet, and P. Rossi for fruitful discussions, and to J. Leterrier for valuable comments on the manuscript. Detailed and constructive reviews by G. Dias and O. Eklund are gratefully acknowledged. This work benefited from financial support from the Agadir University, CNRS-CNR (grant 1021/95), French Ministry of Foreign Affairs (A.I. 98/163/STU) and CRPG-CNRS. This is CRPG contribution no. 1513.

References

Aït Malek, 1997Aït Malek, H., 1997. Pétrologie, géochimie et géochronologie U–Pb d'associations acide–basique : exemples du SE du Velay (MCF) et de l'Anti-Atlas occidental (Maroc). Unpubl. Thesis, INPL Nancy. 268 pp.

Aït Malek et al., 1998H. Aït Malek, D. Gasquet, J.M. Bertrand and J. Leterrier , Géochronologie U–Pb sur zircon de granitoïdes éburnéens et panafricains dans les boutonnières protérozoïques d'Igherm, du Kerdous et du Bas Drâa (Anti-Atlas occidental, Maroc). *C. R. Acad. Sci. Paris* **327** (1998), pp. 819–826.

Anderson and Smith, 1995J.L. Anderson and D.R. Smith , The effects of temperature and f_{O_2} on the Al-in-hornblende barometer. *Am. Mineral.* **80** (1995), pp. 549–559.

Arth and Hanson, 1975J.G. Arth and G.N. Hanson , Geochemistry and origin of the early Precambrian crust of northern Minnesota. *Geochim. Cosmochim. Acta* **39** (1975), pp. 325–362.

Barbey et al., 1999P. Barbey, C. Marignac, J.M. Montel, J. Macaudière, D. Gasquet and J. Jabori , Cordierite growth textures and the conditions of genesis and emplacement of crustal granitic magmas: the Velay granite complex (Massif Central, France). *J. Petrol.* **40** (1999), pp. 1425–1441.

Ben Othman et al., 1984D. Ben Othman, S. Fourcade and C.J. Allègre , Recycling processes in granite–granodiorite complex genesis: the Querigut case studied by Nd–Sr isotopic systematics. *Earth Planet. Sci. Lett.* **69** (1984), pp. 290–300.

Blundy and Wood, 1991J.D. Blundy and B.J. Wood , Crystal-chemical controls on the partitioning of Sr and Ba between plagioclase feldspar, silicate melts, and hydrothermal solutions. *Geochim. Cosmochim. Acta* **55** (1991), pp. 193–209.

Boher et al., 1992M. Boher, W. Abouchami, A. Michard, F. Albarède and N.T. Arndt , Crustal growth in West Africa at 2.1 Ga. *J. Geophys. Res.* **97** (1992), pp. 345–369.

Charlot, 1982R. Charlot , Caractérisation des événements éburnéens et panafricains dans l'Anti-Atlas marocain. Apport de la méthode géochronologique Rb/Sr. *Notes Mem. Serv. Geol. (Morocco)* **313** (1982) 106 pp. .

Choubert, 1952G. Choubert , Histoire géologique du domaine de l'Anti-Atlas. In: *Géologie du Maroc*Notes Mem. Serv. Geol. (Morocco) **vol. 100** (1952), pp. 75–194.

Choubert, 1963G. Choubert , Histoire géologique du Précambrien de l'Anti-Atlas. *Notes Mem. Serv. Geol. (Morocco)* **162** (1963) 352 pp. .

Clemens and Mawer, 1992J.D. Clemens and C.K. Mawer , Granitic magma transport by fracture propagation. *Tectonophysics* **204** (1992), pp. 339–360.

DePaolo, 1981D.J. DePaolo , Trace element and isotopic effects of combined wallrock assimilation and fractional crystallization. *Earth Planet. Sci. Lett.* **53** (1981), pp. 189–202.

Dias and Leterrier, 1994G. Dias and J. Leterrier , The genesis of felsic–mafic plutonic associations: a Sr and Nd isotopic study of the Hercynian Braga Granitoid Massif (Northern Portugal). *Lithos* **32** (1994), pp. 207–223.

Dias and Leterrier, 1995G. Dias and J. Leterrier , Estudo isotópico Sr–Nd de encaves microgranulares máficos associados a granitoídes tardi-hercínicos da região de Braga—Vieira do Minho (Norte de Portugal): origem e composição dos magmas. *Publ. Mus. Lab. Mineral. Geol., Univ. Porto Mem.* **4** (1995), pp. 711–715.

Evensen et al., 1978N.M. Evensen, M.J. Hamilton and R.J. O'Nions , Rare-earth abundances in chondritic meteorites. *Geochim. Cosmochim. Acta* **42** (1978), pp. 1199–1212.

Gasquet et al., 1992D. Gasquet, J. Leterrier, Z. Mrini and P. Vidal , Petrogenesis of the Hercynian Tichka plutonic complex (Western Anti-Atlas, Morocco): trace element and Rb–Sr and Sm–Nd isotopic constraints. *Earth Planet Sci. Lett.* **108** (1992), pp. 29–44.

Gilbert et al., 1982M.C. Gilbert, R.T. Helz, R.K. Popp and F.S. Spear , Experimental studies of amphibole stability. In: D.R. Veblen and P.H. Ribbe, Editors, *Amphiboles: Petrology and Experimental Phase Relations* *Rev. Mineral.* **vol. 9B**, Mineral. Soc. Am., Washington, DC (1982), pp. 229–353.

Harrison and Watson, 1984T.M. Harrison and E.B. Watson , The behavior of apatite during crustal anatexis: equilibrium and kinetic considerations. *Geochim. Cosmochim. Acta* **48** (1984), pp. 1467–1477.

Haskin et al., 1968L.A. Haskin, M.A. Haskin, P.A. Frey and T.R. Wildeman , Relative and absolute terrestrial abundance of the rare-earth. In: L.H. Ahrens, Editor, *Origin and the Distribution of Elements* *Int. Ser. Monogr. Earth Sci.*, Pergamon, Oxford (1968), pp. 889–912.

Hassenforder, 1987Hassenforder, B., 1987. La tectonique panafricaine et varisque de l'Anti-Atlas dans le massif du Kerdous (Maroc). Thèse Sc., Univ. Louis Pasteur, Strasbourg, Soc. Géol. Fr., 249 pp.

Hefferan et al., 1992K.P. Hefferan, J.A. Karson and A. Saquaque , Proterozoic collisional basins in a Pan-African suture zone, Anti-Atlas Mountains, Morocco. *Precambrian Res.* **54** (1992), pp. 295–319.

Hogan et al., 1998J.P. Hogan, J.D. Price and M.C. Gilbert , Magma traps and driving pressure: consequences for pluton shape and emplacement in an extensional regime. *J. Struct. Geol.* **20** (1998), pp. 1155–1168.

Holden et al., 1987P. Holden, A.N. Halliday and W.E. Stephens , Neodymium and strontium isotope content of microdiorite enclaves points to mantle input to granitoid production. *Nature* **330** (1987), pp. 53–56.

Hoskin et al., 2000P.W.O. Hoskin, P.D. Kinny, D. Wyborn and B.W. Chappell , Identifying accessory mineral saturation during differentiation in granitoid magmas: an integrated approach. *J. Petrol.* **41** (2000), pp. 1365–1396.

Ikenne et al., 1998M. Ikenne, A. Mortaji, D. Gasquet and J.M. Stussi , Les filons basiques des boutonnières du Bas Drâa et de la Tagragra d'Akka: témoins des distensions néoprotozoïques de l'Anti-Atlas occidental (Maroc). *J. Afr. Earth Sci.* **25-2** (1998), pp. 209–223.

Kretz, 1983R. Kretz , Symbols for rock-forming minerals. *Am. Mineral.* **68** (1983), pp. 277–279.

Leake et al., 1997B. Leake *et al.*, Nomenclature of amphiboles: report of the Subcommittee on Amphiboles of the International Mineralogical Association Commission on New Minerals and Mineral Names. *Eur. J. Mineral.* **9** (1997), pp. 623–651.

Leblanc and Lancelot, 1980M. Leblanc and J.R. Lancelot , Interprétation géodynamique du domaine Pan-Africain (Précambrien terminal) de l'Anti-Atlas (Maroc) à partir de données géologiques et géochronologiques. *Can. J. Earth Sci.* **17** (1980), pp. 142–155.

Leblanc and Moussine-Pouchkine, 1994M. Leblanc and A. Moussine-Pouchkine , Sedimentary and volcanic evolution of a Neoproterozoic continental margin (Bleida, Anti-Atlas, Morocco). *Precambrian Res.* **70** (1994), pp. 25–44.

Martin, 1993H. Martin , The mechanisms of petrogenesis of the Archaean continental crust—comparison with modern processes. *Lithos* **30** (1993), pp. 373–388.

Michard et al., 1985A. Michard, P. Gurriet, M. Soudant and F. Albarède , Nd isotopes in French Phanerozoic shales: external vs. internal aspects of crustal evolution. *Geochim. Cosmochim. Acta* **49** (1985), pp. 601–610.

Nachit et al., 1996H. Nachit, P. Barbey, J. Pons and J.P. Burg , L'Eburnéen existe-t-il dans l'Anti-Atlas occidental marocain? L'exemple du massif du Kerdous. *C. R. Acad. Sci. Paris* **322** Série IIa (1996), pp. 677–683.

Nachit et al., 1999H. Nachit, J. Pons and P. Barbey , Structure and geochemistry of a zoned granodioritic pluton: what about magma–host interactions during emplacement?. In: B. Barbarin, Editor, *The Origin of Granites and Related Rocks 4th Hutton Symp., Abstract. Doc.* vol. **290**, BRGM, Orléans (1999), p. 103.

Paterson et al., 1996S.R. Paterson, T.K. Fowler, Jr. and R.B. Miller , Pluton emplacement in arcs: a crustal-scale exchange process. *Trans. R. Soc. Edinburgh: Earth Sci.* **87** (1996), pp. 115–123.

Pitcher, 1979W.S. Pitcher , The nature, ascent and emplacement of granitic magmas. *J. Geol. Soc. London* **136** (1979), pp. 627–662.

Pupin, 1980 J.P. Pupin, Zircon and granite petrology. *Contrib. Mineral. Petrol.* **73** (1980), pp. 207–220.

Raase et al., 1985 P. Raase, M. Raith, D.K. Ackermann and R.K. Lal, Progressive metamorphism of mafic rocks from greenschist to granulite facies in the Dharwar craton of south India. *J. Geol.* **94** (1985), pp. 261–282.

Rapela and Pankhurst, 1996 C.W. Rapela and R.J. Pankhurst, Monzonite suites: the innermost Cordilleran plutonism of Patagonia. *Trans. R. Soc. Edinburgh: Earth Sci.* **87** (1996), pp. 193–203.

Reiners et al., 1995 P.W. Reiners, B.K. Nelson and M.S. Ghiorso, Assimilation of felsic crust by basaltic magma: thermal limits and extents of crustal contamination of mantle-derived magmas. *Geology* **23** (1995), pp. 563–566.

Saquaque et al., 1989 A. Saquaque, H. Admou, J. Karson, K. Hefferan and I. Reuber, Precambrian accretionary tectonics in the Bou-Azzer-El Graara region, Anti-Atlas, Morocco. *Geology* **17** (1989), pp. 1107–1110.

Scaillet et al., 1998 B. Scaillet, F. Holtz and M. Pichavant, Phase equilibrium constraints on the viscosity of silicic magmas I: Volcanic–plutonic comparison. *J. Geophys. Res.* **103** (1998), pp. 27257–27266.

Spear, 1981 F.S. Spear, An experimental study of hornblende stability and compositional variability in amphibolite. *Am. J. Sci.* **281** (1981), pp. 697–734.

Veloso and Dias, 1995 M.L. Veloso and G. Dias, Estudo químico-mineralógico de enclaves microgranulares máficos associados a granitóides tardi-hercínicos da região de Braga-Vieira do Minho (Norte de Portugal): tipo e mecanismos de hibridação. *Publ. Mus. Lab. Mineral. Geol., Univ. Porto Mem.* **4** (1995), pp. 843–847.

Vigneresse and Clemens, 2000 J.L. Vigneresse and J.D. Clemens, Granitic magma ascent and emplacement: neither diapirism nor neutral buoyancy. In: B. Vendeville, Y. Mart and J.L. Vigneresse, Editors, *Salt, Shale and Igneous Diapirs in and around Europe* *Geol. Soc. London, Spec. Publ.* **vol. 174** (2000), pp. 1–19.

Vigneresse et al., 1999 J.L. Vigneresse, B. Tikoff and L. Améglio, Modification of the regional stress field by magma intrusion and formation of tabular granitic plutons. *Tectonophysics* **302** (1999), pp. 203–224.

Villeneuve and Cornée, 1994 M. Villeneuve and J.J. Cornée, Structure, evolution and palaeogeography of the West African craton and bordering belts during the Neoproterozoic. *Precambrian Res.* **69** (1994), pp. 307–326.

Vyhnal et al., 1991 C.R. Vyhnal, H.Y. McSween, Jr. and J.A. Speer, Hornblende chemistry in southern Appalachian granitoids: implications for aluminum hornblende thermobarometry and magmatic epidote stability. *Am. Mineral.* **76** (1991), pp. 176–188.

Watson and Harrison, 1983E.B. Watson and T.M. Harrison , Zircon saturation revisited: temperature and composition effects in a variety of crustal magma types. *Earth Planet. Sci. Lett.* **64** (1983), pp. 295–304.

Wiebe, 1994R.A. Wiebe , Silicic magma chambers as traps for basaltic magmas: the Cadillac Mountain intrusive complex, Mount Desert Island, Maine. *J. Geol.* **102** (1994), pp. 423–437.

Wiebe and Collins, 1998R.A. Wiebe and W.J. Collins , Depositional features and stratigraphic sections in granitic plutons: implications for the emplacement and crystallization of granitic magma. *J. Struct. Geol.* **20** (1998), pp. 1273–1289.

Williamson et al., 1992B.J. Williamson, H. Downes and M.F. Thirwall , The relationship between crustal magmatic underplating and granite genesis: an example from the Velay granite complex, Massif Central, France. *Trans. R. Soc. Edinburgh: Earth Sci.* **83** (1992), pp. 235–245.

Zen and Hammarstrom, 1984E. Zen and J.M. Hammarstrom , Magmatic epidote and its petrologic significance. *Geology* **12** (1984), pp. 515–518.